Mon. Not. R. Astron. Soc. **000**, 000–000 (0000) Printed 2 February 2008 (MN LATEX style file v2.2)

Correlated spectral variability in brown dwarfs

C.A.L. Bailer-Jones⋆
Max-Planck-Institut für Astronomie, Königstuhl 17, D-69117 Heidelberg, Germany

Submitted 2 March 2007; Accepted 27 November 2007

ABSTRACT

Models of brown dwarf atmospheres suggest they exhibit complex physical behaviour. Observations have shown that they are indeed dynamic, displaying small photometric variations over timescales of hours. Here I report results of infrared (0.95–1.64 μm) spectrophotometric monitoring of four field L and T dwarfs spanning timescales of 0.1–5.5 hrs, the goal being to learn more about the physical nature of this variability. Spectra are analysed differentially with respect to a simultaneously observed reference source in order to remove Earth-atmospheric variations. The variability amplitude detected is typically 2–10%, depending on the source and wavelength. I analyse the data for correlated variations between spectral indices. This approach is more robust than single band or χ^2 analyses, because it does not assume an amplitude for the (often uncertain) noise level (although the significance test still assumes a shape for the noise power spectrum). Three of the four targets show significant evidence for correlated variability. Some of this can be associated with specific features including Fe, FeH, VO and KI, and there is good evidence for intrinsic variability in H_2O and possibly also CH_4. Yet some of this variability covers a broader spectral range which would be consistent with dust opacity variations. The underlying common cause is plausibly localized temperature or composition fluctuations caused by convection. Looking at the high signal-to-noise ratio stacked spectra we see many previously identified spectral features of L and T dwarfs, such as KI, NaI, FeH, H_2O and CH_4. In particular we may have detected methane absorption at 1.3–1.4 μm in the L5 dwarf SDSS 0539−0059.

Key words: stars: low-mass, brown dwarfs – stars: variables: other — stars: individual: SDSSp J053951.99-005902.0 — stars: individual: 2MASS J05591914-1404488 — stars: individual: SSSPM J0829-1309 — stars: individual: 2MASS J08472872-1532372 – methods: data analysis

1 INTRODUCTION

Numerous observational studies over recent years have revealed photometric variability in old brown dwarfs and very low mass stars with spectral types late M, L and T (collectively ultracool dwarfs, or UCDs) (e.g. Gelino et al. (2002), Koen et al. (2004)). The variability is always of low amplitude (a few tens of millimagnitudes) and often nonperiodic, leading some authors to interpret this as a result of intrinsic atmospheric variability (Bailer-Jones & Mundt (2001)) rather than a rotational modulation. The idea here is that, while UCDs are rapid rotators (Mohanty & Basri (2003), Bailer-Jones (2004)) with likely periods of 3–10 hrs, heterogeneous variations in opacity on a shorter timescale could account for the observed signature. In an earlier review of the literature, Bailer-Jones (2005) estimated that 40% of UCDs are variable, although this may be a lower limit due to limited observations, plus the fact that a given UCD is not always variable. For a more recent review and discussion see Goldman (2005).

Among young (1–10 Myr) low mass stars and brown dwarfs (with mid and late M spectral types) variability is also common (e.g. Joergens et al. (2003)), with also about $\sim 40\%$ of objects variable, but this is typically periodic and with larger amplitudes of up to a few tenths of a magnitude (reviewed in Bailer-Jones (2005)). This is similar to that seen in (low mass) T Tauri stars, where the variability is related to cool spots. For the older, cooler objects considered here the physical mechanism behind the variability is less clear, because the predicted neutrality of their atmospheres inhibits formation of magnetically-cooled regions. Local opacity variations could arise from local temperature or composition variations, one or both of which could be caused from convective flows of matter to/from the deeper, opaque regions of the atmosphere.

To investigate this further, multiband monitoring is required. Bailer-Jones (2002) (hereafter BJ02) used synthetic UCD spectra to predict the variability signature due to spots

⋆ Email: calj@mpia-hd.mpg.de

and dust clouds and used these to analyse spectral time series of an L1.5 dwarf. While there was no evidence for variability in a single channel, there was a suggestion of correlated variations which were consistent with dust. Nakajima et al. (2000) found a suggestion of water variability in a T dwarf, while Clarke et al. (2003) found no variability in the dust-sensitive band heads of TiO, CrH and FeH of the L2V Kelu-1.

Here I report on infrared spectrophotometric monitoring of four UCDs. This is an extension of a pilot study in BJ02. The objective is to identify which (if any) parts of the spectrum are most variable and, moreover, which regions show significant correlated variability with one another. If the correlated variations can be traced to specific molecules (e.g. water, methane, FeH) or dust-sensitive regions, then not only is this a more robust detection of intrinsic variability (as opposed to instrumental or telluric artefacts), but may provide some clues to the nature of the atmospheric variations.

2 DATA ACQUISITION AND REDUCTION

2.1 Targets

Targets were chosen based on their observability (RA and Dec), brightness and spectral type. There had to be a bright, nearby star to act as a reference (but not too bright or close), although this was met by most candidates. The targets are listed in Table 1. 2MASS 0559 was monitored by Enoch et al. (2003) who found no Ks-band variability above an amplitude of 0.1 mag over a timescale of a few days. Tinney et al. (2003) measured its parallax and suspected it to be a binary on account of its apparent overluminosity (i.e. compared to models), although Burgasser et al. (2003) found no evidence for binarity from HST observations. SDSS 0539 was monitored in the I-band by Bailer-Jones & Mundt (2001) who found it to be significantly variable (p = 3e-5) at a period of 13.3 ± 1.2 hrs (20σ detection in the periodogram).

2.2 Observations

Infrared spectra were obtained with SOFI on the 3.5m NTT ESO telescope on La Silla, Chile. The field-of-view was $4.98' \times 4.98'$ and the pixel scale $0.292''$/pix. I used the blue grism with a dispersion of 0.696 nm/pix which imaged the spectral range 0.95–1.64 μm in first order. With a spectrograph slit width of $2''$ this delivered a nominal resolving power of 300, corresponding to a spectral profile with full width at half maximum (FWHM) of 3.3 nm at 1 μm (5 pixels) and 5.3 nm at 1.6 μm (8 pixels).

The observing procedure is similar to that used in BJ02. Each target was monitored continuously for a few hours, dithered between two positions on the slit (separated by about 1 arcmin). At each position a set of three 60s exposure images was obtained (each comprising three co-added 20s exposures). The total time required for the two consecutive dither positions (which will form a "paired spectrum") is 7.8 minutes. A nearby reference star of comparable brightness was placed in the slit and spectra acquired simultaneously. Data were acquired over two nights in January 2004 as listed in Table 2. Although mostly clear, some thin cloud was present at times.

Table 2. Observing log. The normal spacing between consecutive paired spectra is 7.8 minutes. The FWHM refers to the width of the extracted spectra (which is generally larger than the image seeing).

UT range	name	# paired spectra	airmass	FWHM arcsec
	Night 1 (2004 January 10 UT)			
01:28 – 03:42	SDSS 0539	16	1.14–1.20	0.9–1.3
03:56 – 09:22	SSSPM 0828	30	1.04–1.56	0.9
	Night 2 (2004 January 11 UT)			
01:20 – 05:06	2MASS 0559	26	1.04–1.18	0.9
05:30 – 09:20	2MASS 0847	25	1.04–1.39	0.9–1.5

2.3 Image reductions and spectral extraction

The three consecutive images at each of the two positions were summed. The difference between these removes most of the sky background and gives the two *difference images*, each with an effective exposure time of three minutes. After flat fielding (see below), the spectra were extracted with the APSUM package in IRAF. A residual background on either side of the spectrum is computed and subtracted. The spectra are wavelength calibrated using Xenon arc lamps. A 16-line fit with a cubic Chebyshev polynomial produced an RMS fit of 0.13 nm, which is about 1/30 the spectral FWHM. Each spectrum is cubic spline interpolated to a uniform wavelength scale (0.696 nm/pix) with 1028 pixels. The spectra are not flux calibrated and the flux scale is proportional to photon counts.

Because the seeing disk was typically smaller than the slit width, successive spectra could show small shifts in the dispersion direction. This would produce variations in the wavelength zero point. These I determined by cross correlating each extracted spectrum against the first in the series (masking out low SNR regions). For SSSPM 0828, the standard deviation in the shifts was about 0.4 pixels. As the wavelength calibration is only accurate to 0.2 pixels, and because the spectra will anyway be binned (see below) I decided not to apply zero point offsets.[1]

A sky spectrum at the position of the target and reference stars is extracted directly from the raw (not flat fielded or differenced) images, using the extraction apertures already defined. These are used together with the extracted spectra, readout noise estimates and the assumption of Poisson noise from source and sky to provide an estimate of the noise at each wavelength (the *sigma spectrum*). This is used only to calculate the χ^2 spectra.

[1] Reductions of SSSPM 0828 with and without these zero point wavelength shifts were compared: There was no qualitative difference in the results.

Table 1. Targets observed. The reference is the discovery paper and provides the spectral type and full name. The photometry is from 2MASS from the archive compiled by Kirkpatrick (2003).

name	Full name	SpT	J	reference
SDSS 0539	SDSSp J053951.99-005902.0	L5	14.03	Fan et al. (2000)
2MASS 0559	2MASS J05591914-1404488	T5	13.80	Burgasser et al. (2000)
SSSPM 0828*	SSSPM J0829-1309	L2	12.80	Scholz & Muesinger (2002)
2MASS 0847	2MASS J08472872-1532372	L2	13.51	Cruz et al. (2003)

* The discoverers (unconventionally) round off the target's RA coordinate (which they report as J2000 08h 28m 34.11s) to the nearest minute in assigning a name, rather than truncating it. I avoid this, resulting in the shortened name SSSPM 0828.

2.3.1 Flat fielding

Flat fielding of the difference images was performed to correct for both pixel-to-pixel sensitivity variations and global illumination variations. A global correction is necessary *in the spatial direction* because the stars are observed in two different dither positions. Two types of flat field calibrations were obtained: (1) Internal flats, using a lamp inside the instrument. The light path is very short (so there is little atmospheric absorption), but the illumination is quite different from the telescope pupil illumination (i.e. it's not "flat"). (2) External flats using a flat-field screen in the dome, which have the inverted problem (appropriate pupil illumination but long path length). The internal flats provide the appropriate high frequency correction and the external flats the low frequency one. I combine these by first removing the global variation from the internal flat by dividing it by its 2D cubic spline fit (with five knots in each dimension) and then multiplying the result by the same order fit to the external flat (then normalize). (A similar procedure was used by Bailer-Jones & Mundt (2001) for optical imaging.)

It is not possible to achieve an accurate flat field correction in the dispersion direction, because of the broad absorption features in the external flat (precluding an accurate definition of the global fit). However, because the sources are not displaced in the dispersion direction between the two dither positions, and because we are only using these data to look for temporal variations in the spectra, an accurate correction is not required.

2.4 Spectral rectification, pairing and binning

A *relative spectrum* is the target spectrum divided by the reference spectrum. On the assumption that the reference star shows no variations on the timescales of interest, this should remove variations due to the Earth's atmosphere. There were, however, still variations with time of the integrated flux of the relative spectra. A similar problem was found in BJ02, where it was concluded the problem was differential light losses at the slit. I remove this by dividing from each relative spectrum its integrated flux ("rectification"): this puts all relative spectra on a common scale. Because the full spectral range includes the deep telluric absorption band between the J and H bands, the flux was integrated only over the regions 0.990–1.316 μm and 1.489–1.629 μm.

Some analyses are later performed on the non-relative spectra of the target or reference spectra (also rectified by division of the integrated flux). These will be referred to as *direct spectra*.

Plotting the flux vs. time for a given wavelength bin showed, for some bins, a small scale "zig-zag" variation in flux between consecutive spectra (i.e. the two dither positions). This may be a residual flat fielding problem (or other detector issue). This is removed by simply averaging the two spectra formed at the two consecutive dither positions to give the *paired spectrum*.[2] All spectra referred to from now on are rectified, paired spectra.

The SNR per pixel in a relative spectrum of SSSPM 0828 is typically 17 (ranging from 13–20 outside of the strong water absorption band). This is increased (at the expense of spectral resolution) by binning the spectra, specifically, by taking the median of successive blocks of B pixels. Taking the median rather than the mean almost entirely removes cosmic rays and bad pixels. Note that I *bin* rather than *smooth* in order that the binned pixels be independent. All spectral plots in this paper are for $B = 1$ (i.e. 0.696 nm/pix) and the corelation analysis is done at $B = 20$.

3 ANALYSIS

Most previous UCD variability analyses have used just a single photometric band; the presence of variability is established using a statistic (typically χ^2 or the F-statistic) which compares the observed variations to those expected by the null hypothesis (i.e. the noise). (Koen (2004) discusses other statistics.) This is repeated here, but now using all of the 1028 bands in the unbinned spectra. The main contribution of the present work, however, is to look for *correlated* variations between spectral bins, independently of estimated errors. This is done on the binned spectra (to improve the SNR), with attention paid in particular to known chemical features or potentially sensitive indices. The assumption is that some intrinsic variability will be coherent across different parts of the spectrum. The method is outlined using SSSPM 0828 and then the results for each target summarized in section 4.

[2] Dithering the telescope was performed in order to improve sky subtraction. Given the difficulties of flat fielding to sufficient precision and the possibility of other detector variations it is not clear that dithering bestowed a net advantage. Given a telescope with excellent guiding and observations performed under stable weather conditions, it is probably better to observe bright targets without dithering at all.

3.1 Spectra

The series of 30 relative spectra in the time series of SSSPM 0828 is shown in Fig. 1.[3] The median target (direct) and relative spectra are shown in Fig. 2 (panels A and B). Panel (C) shows the amplitude of the variations in the form of the median absolute deviations (MAD) and panel (D) the χ^2 spectrum, both for the relative spectrum. The MAD is a more robust version of the standard deviation, and includes a correction factor to achieve asymptotic consistency with the standard deviation of a normal distribution. The χ^2 spectrum (see section 2.3) identifies pixels with a large measured variation compared to the variation predicted from just the noise model. Thus the saturated telluric water absorption band between 1.31 and 1.49 μm (and to a lesser extent the weaker one at 1.10–1.16 μm) shows a large MAD in Fig. 2, yet a low χ^2 because the estimated noise is also large.

Fig. 3 shows the 0.95–1.32 μm region of the median relative spectra for all four targets.

3.2 Correlation matrices

3.2.1 Definition

Conclusions drawn from the χ^2 spectrum alone are sensitive to the estimated errors. As discussed by Bailer-Jones & Mundt ((1999)), these are difficult to estimate accurately, because the basic prescription based on photon and readout noise neglects other sources. I overcome this limitation by looking for variability correlations in wavelength space. I calculate the (Pearson) correlation coefficients between all pairs of (binned) pixels across the whole time series. These are plotted as a matrix in Fig. 4, with the colour scale indicating the modulus of the correlation coefficients, $|\rho_{i,i'}|$. 1.0 indicates perfect correlation (or anti-correlation) and 0.0 no correlation. The matrix is of course symmetric with unit values on the leading diagonal. By plotting $|\rho_{i,i'}|$ rather than $\rho_{i,i'}$ the plots do not distinguish between correlations and anti-correlations, which eases comparison with the matrix for random spectra (see below). We will see from the histograms in the next section that all targets have a bias towards stronger positive correlations, although SDSS 0539 also shows significant anti-correlations. We clearly see structure in the matrix, with some regions of high correlation. The correlation matrix at higher and lower binning factors shows similar patterns. The presence of structure suggests correlated variations in the UCD. (The issue of autocorrelation is discussed in section 3.2.4).

3.2.2 Control sample: random spectra

To determine whether the correlations are statistically significant we require a control. For this I generate a series of S random spectra in which each pixel is drawn at random from a $\mathcal{N}(0,1)$ distribution, where S is the number of spectra in the series (S=30 for SSSPM 0828). An example of one such correlation matrix is shown in Fig. 5. Note that its properties are independent of the mean and standard deviation used. Comparing this with Fig. 4 we see that the latter shows many more cells of significant correlation. The same qualitative conclusion can be drawn from the frequency distribution (histograms) of these correlation coefficients (Fig. 6): The distribution for the UCD spectra is significantly broader and has more positive correlations than that for the random spectra.

3.2.3 Statistical significance of correlations

We can quantify the significance of variations from these control spectra and their correlation matrices. By looking at the (cumulative) distribution of the correlation coefficients for large numbers of random spectra we can derive confidence intervals (this could also be done analytically).

The expectation value of $\rho_{i,i'}$ is of course zero. The cumulative distribution, $C(\rho_{i,i'})$, of the correlation coefficients is the probability that $\rho_{i,i'}$ is less than some value under the null hypothesis of Gaussian random variations. We are interested in significant positive or negative correlations, so I make a two-sided test at the 0.1% confidence level. As the standard deviation of $\rho_{i,i'}$ (Fig. 6, bottom) is smaller for larger S, this is done separately for each target. A set of S spectra is generated and the confidence interval determined. This is repeated many times (ten thousand) and the average confidence interval determined (a limiting cumulative distribution is shown in Fig. 7). The 0.1% confidence limits are (see Table 2): ± 0.72 ($S = 16$); ± 0.62 ($S = 25$); ± 0.61 ($S = 26$); ± 0.57 ($S = 30$). Under the assumptions adopted, values of $|\rho_{i,i'}|$ larger than these indicate significant correlations.

These confidence limits are based on Gaussian distributions (the random spectra). The variations in the observed spectra may not be Gaussian, but in the absence of a better model this is a useful baseline. As a check I also calculated the correlation matrices using the non-parametric Spearman's rank correlation coefficient. The matrices showed very similar patterns, albeit with slightly smaller absolute values. The advantage of this correlation analysis over much previous work on UCD variability is that it makes no assumptions about the values of the parameters of the noise model. In contrast, the χ^2 statistic must assume an amplitude for the noise level, and compare observed variations to this to test for significance.

3.2.4 Autocorrelation

In principle autocorrelation in the time series of a single (binned) pixel could produce spurious cross correlations between pixels (e.g. Chatfield (1996)). However, it turns out that the level of autocorrelation is rather low: Inspection of the correlograms shows that the degree of autocorrelation is no higher (or lower!) than that seen in the control spectra. This is the case for the full range of time lags. Even in the region around 1.05 μm in SSSPM 0828 (Fig. 4), for example, where we see large cross correlation coefficients, these pixels show a low level of autocorrelation. Both the control spectra and the brown dwarfs spectra can show non-zero autocorrelation because noise can correlate by chance. This is taken

[3] Movies of the time series are available with the online edition of this article. The data themselves are available from the author upon request.

into account when defining confidence intervals based on the control spectra.

3.2.5 Significantly correlated regions

With a binning factor of $B = 20$, there are $N = 51$ independent binned pixels and thus $N \times (N-1)/2 = 1275$ correlation coefficients. With the 0.1% confidence intervals we would expect one significant value just by chance. Partly for this reason I adopt a conservative margin on top of the formal confidence limits derived above, and define significantly correlated regions to be those with $|\rho_{i,i'}| > 0.8$. Table 3 lists those wavelength bins which show a significant correlation with at least one other bin: For each spectrum, all bins are listed which have $|\rho_{i,i'}| > 0.8$ in the binned relative spectra. 2MASS 0847 has no significantly correlated bins. Several bins show a significant correlation with more than one other bin, as can be seen from the total number of correlated pairs listed at the bottom of the table. The binned spectra have 51 binned pixels, and there are 39 distinct entries in the table. That is, 12 spectral bins do not have significant correlations in any spectrum. The column "feature" lists atomic and molecular features identified in L and T dwarfs which are coincident with the given bins. Many of these have been taken from McLean et al. (2003) and Cushing et al. (2005). There are some additional, weaker features which have not been listed. Many of these cannot be seen at the resolution used in the present work (although unresolved lines/bands could of course still be variable). For example, Cushing et al. identified many FeH features between 0.998 and 1.085 μm, and methane absorption extends over 1.15–1.25 μm.

I discuss these significant correlations for each object in section 4.

3.2.6 Correlations are not due to OH lines

An imperfect sky subtraction could, in principle, lead to variability in the OH lines, and to examine this the stronger lines are also listed in Table 3. While some of the variable regions coincide with OH lines, many bins at the location of OH lines are not variable. Quantitatively, of the 20 strong OH lines present in the observed wavelength region, 11 are at wavelengths which show no variability in any of the observed UCDs (so are not listed) and these are not simply the weaker OH lines. Furthermore, none of the correlated bands in 2MASS 0559 and none of the more significantly ($|\rho_{i,i'}| > 0.9$) correlated bands in SSSPM 0828 are associated with OH features. SDSS 0539 has quite a few correlated bins, but of those listed in Table 3 which correspond to OH lines, the bins they correlate with mostly do *not* contain OH lines: Of the 19 pairs with $|\rho_{i,i'}| > 0.9$ only two have OH lines in both bins. In conclusion, while we cannot rule out telluric OH lines as causing *some* apparent variability, it is certainly not responsible for a significant fraction of it.

Table 3. Wavelength bins (in nm) which show a significant correlation ($|\rho_{i,i'}| > 0.8$) with at least one other bin. Those in bold have $|\rho_{i,i'}| > 0.9$. This is obtained for a B=20 binning where the bin width is 13.2 nm. The column "feature" lists atomic and molecular features identified in L and T dwarf spectra (although not necessarily present at all spectral types) which are coincident with the given bins and thus potentially responsible for the detected correlated variability. Also indicated in this column are telluric OH lines. A question mark ("?") indicates no specific feature. The total number of *pairs* of bins with $|\rho_{i,i'}| > 0.8$ is given in the penultimate table row and the number with $|\rho_{i,i'}| > 0.9$ is in the final row.

Feature	SDSS 0539	2MASS 0559	SSSPM 0828	2MASS 0847
H_2O		942		
H_2O, VO		955		
H_2O	969			
FeH H_2O	**983**			
Fe FeH CrH	997		997	
?			**1011**	
?	1025		**1025**	
?	1039		**1039**	
VO	**1053**		**1053**	
?	1066		**1066**	
? OH	**1080**		1080	
TiO OH	**1094**			
?	1108		1108	
H_2O			1122	
KI	1177			
Fe FeH	1191			
FeH	1205			
FeH OH	1219			
KI	1247			
?	**1261**			
?	**1275**		1275	
CH_4 TiI OH	**1288**		1288	
CH_4 H_2O OH	**1302**		1302	
CH_4 CaI AlI	**1316**			
H_2O		1344		
H_2O		1441		
H_2O	**1469**			
H_2O	1483			
H_2O	**1497**			
KI	1511		1511	
KI OH	**1524**		1524	
?	1538		1538	
?	**1552**		1552	
?	**1566**		1566	
FeH OH	**1580**			
FeH	**1594**			
CH_4 OH	**1608**			
CH_4 OH	1622			
CH_4	**1635**			
N($\|\rho_{i,i'}\| > 0.8$)	114	4	23	0
N($\|\rho_{i,i'}\| > 0.9$)	**19**	**0**	**10**	**0**

4 RESULTS

4.1 SSSPM J0829-1309 (SSSPM 0828)

The direct and relative spectra of the L2 dwarf SSSPM 0828 in Fig. 2 clearly show the presence of the KI doublets at 1169/1178 nm and 1244/1253 nm as well as the FeH Wing-Ford band at 990–994 nm (McLean et al. (2003)). A zoom of this region is shown in Fig. 3. The absorption line at 1140 nm is probably the unresolved NaI doublet at 1138/1141 nm. We see a large absorption feature centered at 1199 nm, which is most likely due to the FeH band head at 1194 nm, possibly blended with an Fe line at 1197 nm. There is marginal indi-

cation of the AlI lines at 1313 nm (perhaps blended with CaI at 1314 nm) and 1315 nm, but no sign of the MnI (1290 nm) or RbI (1323 nm) lines. The feature around 1517 nm is probably KI. Comparing the continua of the target and relative spectra (panels A and B), we see that, in this case, the absorption band between 1.1 and 1.16 micron must be almost entirely due to telluric absorption, because it is not present in the relative spectrum. This is not the case for the wider band between 1.31 and 1.49 μm, however, where we still see significant absorption in the relative spectrum. This is clear evidence for the presence of water in this L2V object.

We see a resolved peak in the spectrum at 1282 nm. It is present in the relative spectra of all four targets. This coincides with the wavelength of the Paschen β line, identified by Cushing et al. (2005) in the spectrum of Arcturus (K1.5) and M dwarfs down to M7. Inspection of the direct reference spectra shows an absorption feature at this wavelength. If all of the reference stars are K to mid M dwarfs (not implausible), it would be intrinsic to them, not present in the target spectra, and therefore would show up as a peak in the relative spectrum. Alternatively this peak could be the "continuum" between two absorption features: the absorption on the red side is plausibly caused by TiI at 1285 nm. TiI is dominant in its monatomic form above atmospheric temperatures of 2500 K, although such layers are below an optical depth of unity for $T_{\rm eff} > 1800$ and 2000 K in the dusty and cond models (respectively) of Allard et al. (2001) (their Figs. 5 and 6). At the lower temperatures higher in the atmosphere Ti becomes increasingly locked into TiO, finally being removed as $CaTiO_3$ at 1957 K (Lodders (1999)).

The correlation matrix (Fig. 4) shows quite a few regions with high correlation, 17 with $|\rho_{i,i'}| > 0.8$ (Table 3). Ten different pairings of five binned pixels show correlations with $|\rho_{i,i'}| > 0.9$, all lying in the range 1010–1070 nm. Some of the $|\rho_{i,i'}| > 0.8$ pixels are coincident with known features, including Fe, FeH, VO, KI and water, and some also have statistically significant χ^2 values. It is interesting that the 17 bins are grouped into five contiguous regions. In conclusion, while we have evidence for significant correlated variability, it is not restricted to readily-identifiable features. The variability could be caused by dust or molecules (which would effect the broader "continuum" rather than lines), for example FeH or water (methane we may want to rule out a priori based on the spectral type).

4.2 2MASS J05591914-1404488 (2MASS 0559)

The target and relative spectra of this T5 dwarf (Fig. 8) show features typical of UCDs, in particular the KI doublets at 1169/1178 nm and 1244/1253 nm, as with SSSPM 0828 (see also Fig. 3). A feature which may be the NaI doublet is barely visible at 1138/1141 nm. The deeper feature near to this is actually centered on 1133 nm (and there is another broader one at 1143 nm). The FeH Wing-Ford band can clearly be seen at 990–994 nm. The putative FeH/Fe feature at 1199 nm seen in SSSPM 0828 is barely visible. We see a strong absorption band extending redwards from about 1.31 nm out to 1.5–1.6 μm. It is much deeper and extends bluer than the absorption in SSSPM 0828 (an L2). This is almost certainly due to water and methane, and as it is seen in both the target and the relative spectra it is certainly intrinsic to the target. The "ripples" superimposed on this may be many weak absorption features. The absorption band redwards of 1.6 μm is likely due to methane; it is entirely lacking in the SSSPM 0828 spectrum.

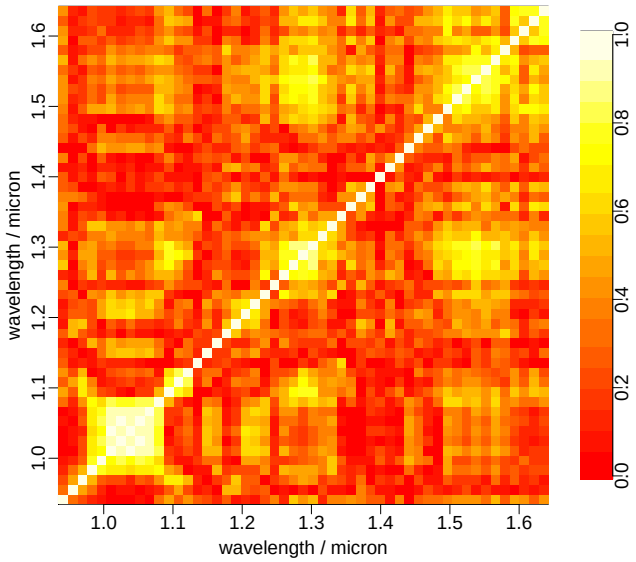

Figure 4. Correlation matrix for the relative spectra of SSSPM 0828 with a binning factor of 20. The absolute values of the correlation coefficients are shown.

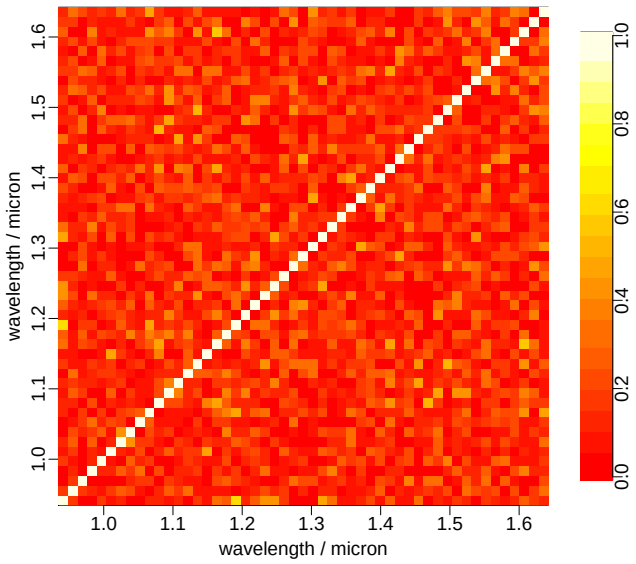

Figure 5. Correlation matrix for a series of random spectra. The same dispersion function (and binning) has been used as for the science spectra. This example uses a set of 30 spectra (the same as SSSPM 0828).

We see another deep absorption feature between 1.08 and 1.2 μm. It again extends much further to the red than the similar band in SSSPM 0828 and could again be increased water absorption in the atmosphere of 2MASS 0559. Note that just because the telluric water band causes large variations (panel C) between 1.35 and 1.40 μm, these variations are not necessarily significant (panel D), because of

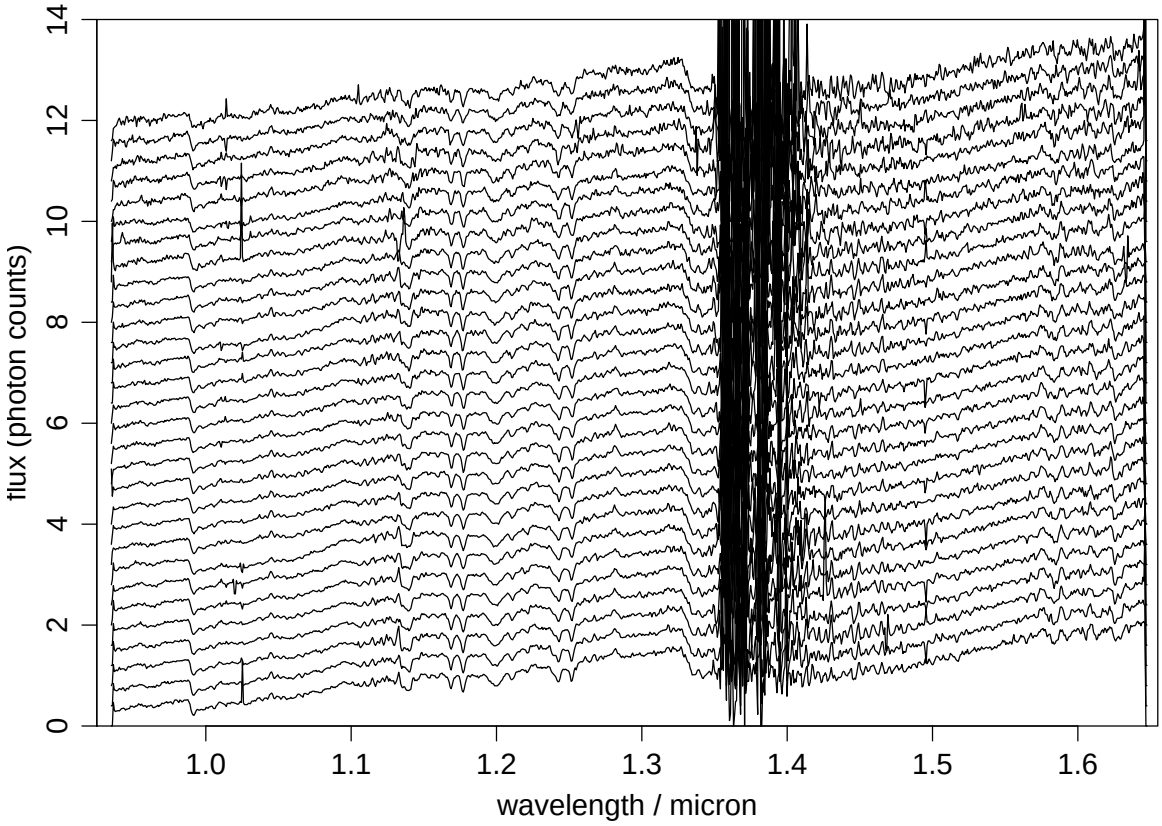

Figure 1. The time series of the (unbinned) relative spectra for SSSPM 0828. Time increases up the plot and the spectra have been offset. The spacing between consecutive spectra is typically 7.8 min. Cosmic rays and bad pixels have not been removed here.

the larger predicted noise. A number of the significant peaks in the χ^2 spectrum are due to cosmic rays (e.g. 1.089, 1.184 and 1.258 μm) or bad/hot pixels (e.g. 1.011, 1.025, 1.495 μm) because we see them in just one spectrum or at one of the two detector positions (respectively).

The correlation matrix (Fig. 9) and histogram (Fig. 10) show a few regions of high correlation (when compared to the random matrix). Above the threshold $|\rho_{i,i'}| > 0.8$ there are four binned pixels (Table 3), all of which coincide with water features. This is discussed further in section 4.6. Whether or not the lack of (or lower level of) correlated variability in other water bands in 2MASS 0559 is consistent with this requires a more detailed analysis of the water spectrum.

4.3 SDSSp J053951.99-005902.0 (SDSS 0539)

The spectra for this L5V object are shown in Fig. 11 and Fig. 3. Although a later type than SSSPM 0828, many of the features are common, so see section 4.1 for a discussion. In SDSS 0539 we again see a non-saturated water band in the relative spectrum. Within this, we see two conspicuous absorption features, one centered at 1362 nm and another at 1371 nm. Similar features are seen in SSSPM 0828 at the same position (to within $\pm$1 nm). This may be genuine structure within the water absorption band, although this region is quite noisy due to low photon counts from the source.

We see that the strength of this absorption band redward of 1.31 μm is intermediate between that seen in the two L2 dwarfs (SSSPM 0828 and 2MASS 0847) and the T5 dwarf (2MASS 0559). As the depth of the latter is due to both water and methane, this could indicate the presence of some methane absorption in SDSS 0539, an L5 object. Methane absorption has been observed in late L dwarfs before, e.g. by Nakajima et al. (2001) in a L6.5V at 1.62 and 1.67 μm and by Schweitzer et al. (2002) at 2.2 and 3.3 μm (L6–L8), but not at this particular band.

The χ^2 spectrum shows some evidence for variability. In their I-band monitoring program, Bailer-Jones & Mundt (2001) found SDSS 0539 to be significantly variable and even detected a significant period at 13.3 ± 1.2 hrs.

The correlation matrix (Fig. 12) shows, in comparison to the previous two objects, significantly more highly correlated binned pixels, as the histogram also makes clear (Fig. 13). 33 distinct binned pixels are significantly correlated, 18 of these with $|\rho_{i,i'}| > 0.9$ (see Table 3). While the evidence for correlated variability is clear, it is not obviously connected to a few specific chemical elements. Many of the correlated binned pixels are contiguous, which points to something with a broad spectral signature being respon-

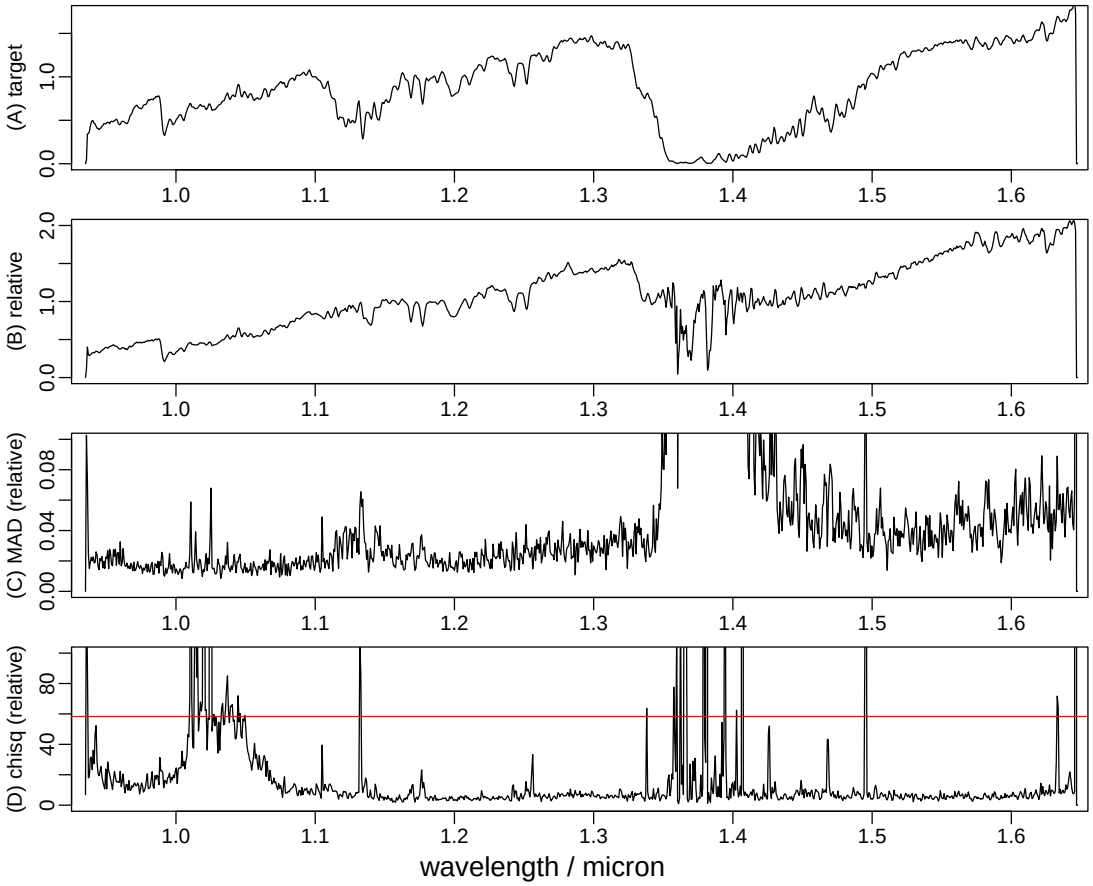

Figure 2. Spectra of the L2 dwarf SSSPM 0828 (unbinned at a dispersion of 0.696 nm/pix, some 1028 pixels). The flux scale is proportional to photon counts (not energy). From top to bottom: (A) The median target spectrum; (B) the median relative spectrum (median of target divided by reference at each epoch). Because both are rectified by dividing by the integrated flux (see section 2.4) the vertical scale is dimensionless. (C) The median absolute deviation in the relative spectrum (a robust version of the standard deviation); (D) The χ^2 spectrum. In this bottom panel, points above the horizontal line are variations beyond the estimated errors with a confidence of 99.9% or more per pixel.

sible, such as solid or liquid particulates ("dust"). Several regions are in common to SSSPM 0828. One may be a little skeptical with the extent of variability, given that this is the faintest object and the spectra are quite noisy. In theory, lower SNR data does not give rise to more significant correlations. On the contrary, the larger noise would dilute any intrinsic correlations. Moreover, the object with the second most correlated binned pixels in the sample of four, SSSPM 0828, is by far the brightest.

Of the four targets, SDSS 0539 is the only one to show significant *anti*correlations, with ten pairs fulfilling the criterion $\rho_{i,i'} < -0.8$. Of these, six involve the bin centered at 1191 nm, which covers Fe and FeH features (Table 3), and this anti-correlates with, amongst others, bins at 1094 nm (TiO) and 1219 nm (FeH). Another pair which can be associated with known features is 1094 nm (TiO) and 1205 nm (FeH). Of course, this is not conclusive evidence that these molecular features are the cause (they sit on top of a continuum, after all). But it would be interesting to see whether dynamic atmospheric models show such anti-correlations.

4.4 2MASS J08472872-1532372 (2MASS 0847)

The spectra Fig. 14 and Fig. 3 show the KI doublets, FeH features and water absorption bands, seen now in all four UCDs observed. We can see the KI line at 1.517 μm identified also in SSSPM 0828. From Figs. 15 and 16 we see no evidence for any correlated variations in the relative spectra: the correlation matrix is hardly distinguishable from the random one in Fig. 5. Interestingly, inspection of the correlation matrices for the direct (non-relative) spectra does reveal correlations within both the target and reference spectra. However, this is misleading, because we are observing through the Earth's variable atmosphere so we expect to see variability in the direct spectra. We furthermore expect this telluric variability to be correlated, e.g. different parts of the water spectrum vary coherently as the water column density varies. Little can be inferred from the direct spectra: A simultaneous reference source must be used (and the analysis performed on the relative spectra, as done throughout this paper). Had we not not done this, we would now be concluding that there are significant correlations in 2MASS 0847. This demonstrates that for variability studies it would be

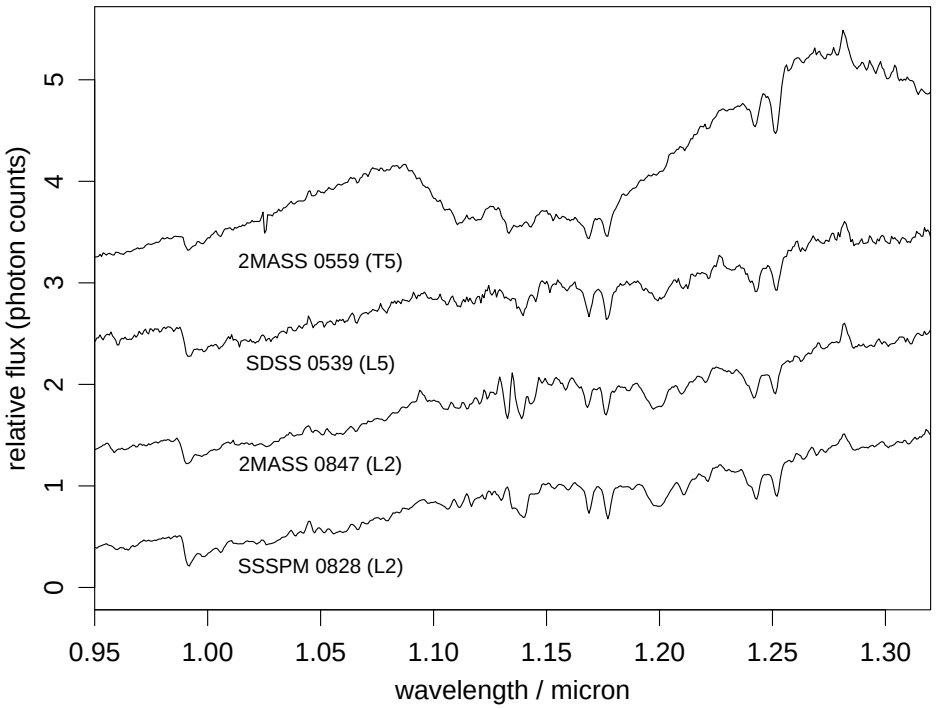

Figure 3. Comparison of the median relative spectra. The spectra have been offset by values of 0,1,2,3 in the vertical scale (these numbers being the zero photon count level for each spectrum). See section 4, in particular section 4.1, for a discussion of the features.

insufficient to correct for a time-averaged telluric absorption using a standard star taken just one or a few times per night.

4.5 Correlations in spectral indices

BJ02 defined some spectral indices intended to be both sensitive to dust cloud variability in UCDs and minimally influenced by (telluric) water absorption. Three of these bands have been formed with the present data (from the rectified, paired, relative spectra – see section 2.4) by integrating over the specified wavelength interval: j1 (1.05–1.09 μm); j2 (1.17–1.30 μm); h1 (1.51–1.64 μm, the red end being truncated with respect to the original definition); h2 (1.51–1.55 μm). For each object, the correlations between these bands are measured. (Note that h1 and h2 overlap so correlations with respect to these bands are not independent.) The only object/bands which show a significant correlation ($|\rho_{i,i'}| > 0.8$) is SDSS 0539 between j1 and h1 with $\rho_{j1,h1} = 0.87$ (and $\rho_{j1,h2} = 0.89$, but this is not independent). From Figs. 2–4 of and Table 2 of BJ02 we see that j1 and h1 would be positively correlated under dust-induced variability. On the other hand, so would j1 and j2, yet this is not seen for SDSS 0539 ($\rho_{j1,j2} = 0.35$).

We may also form flux ratios, j1/j2, j1/h1 etc. which are "unlogged" colours, as the rectification factor cancels out. That is, j1/j2 vs. j1/h1 (for example) examines the correlation of j2 and h1 normalized relative to j1. Of the 10 possible correlations between these per object (excluding h1/h2) we see several significant correlations. For SSSPM 0828 we have $\rho_{j1/j2,j1/h1} = 0.92$ and $\rho_{j1/h2,j1/j2} = 0.92$. The latter is the correlation plotted in Fig. 12 of BJ02 for a very similar spectral type, L1.5V, where $\rho_{i,i'} = 0.83$. Moreover, Fig. 13 of the same paper shows negligible correlation between j2/h2 and j1/j2, and for SSSPM 0828 we have $\rho_{j2/h2,j1/j2} = -0.09$. Thus these two objects show very similar variability patterns. In SDSS 0539 the one significant colour index is $\rho_{j1/j2,j2/h1} = -0.82$. With 2MASS 0559 we have $\rho_{j1/h1,j2/h1} = 0.84$ (0.96 when formed against h2 instead of h1).

This analysis adds support to the conclusion of correlated variability, in particular over a broad spectral range.

4.6 Variability in the 1.31–1.49 μm water band

Nakajima et al. (2000) reported variability in a water band between 1.34 and 1.42 μm in a T dwarf (SDSS 1624+00) from a series of eight spectra taken over a period of 80 minutes. As in the present work, they simultaneously observed a reference star in the spectrograph slit. They claim that the variability is intrinsic to the T dwarf, although it is unclear if this variability is *statistically* significant (such an analysis is not reported) and the authors themselves acknowledge the dependence of this result on a correct estimation of the photometric uncertainties.

From the χ^2 plots in the present paper, this region appears to be significantly variable for 2MASS 0847, SSSPM 0828 and SDSS 0539 (but not for 2MASS 0559). However, the source counts are very low here and error sources not accounted for in the basic noise model may dom-

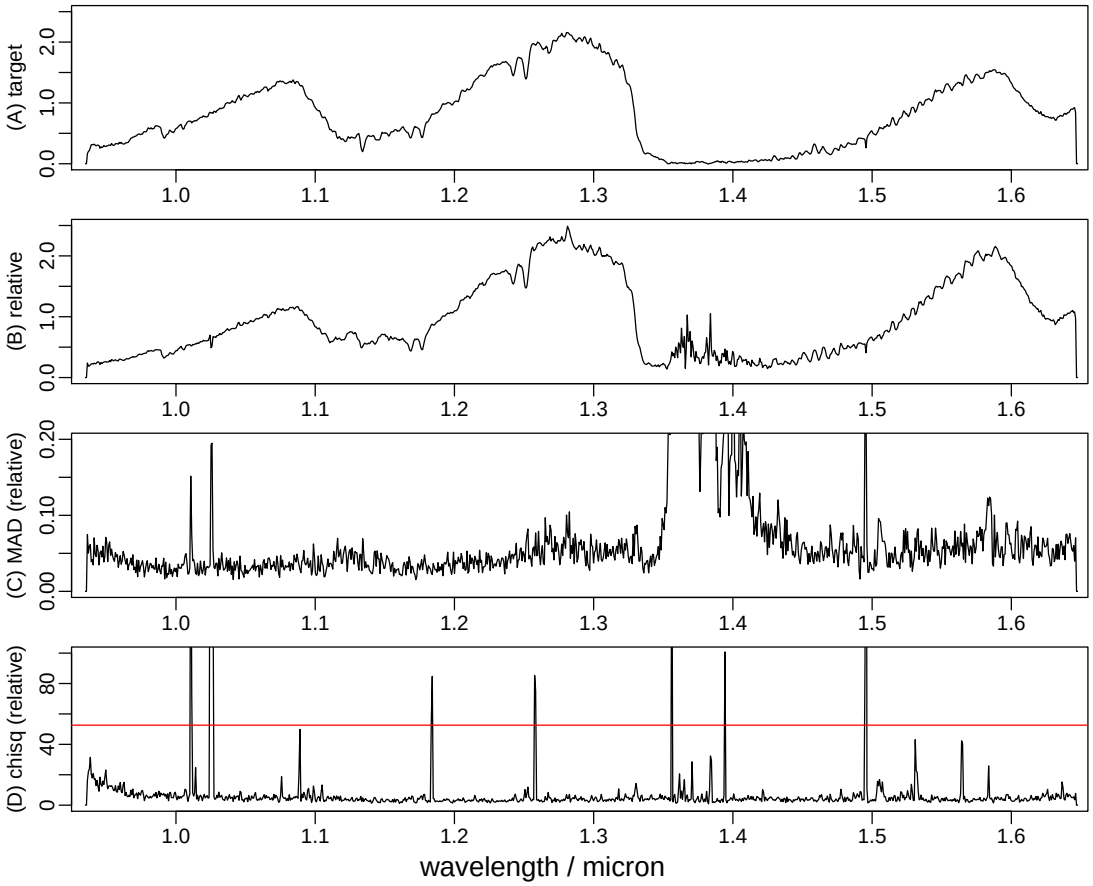

Figure 8. Spectra of the T5 dwarf 2MASS 0559. See caption to Fig. 2.

inate, rendering the χ^2 statistic less reliable. The correlation analysis introduced in the present paper does not assume a noise model for the data. 2MASS 0847 shows no significant correlations in this band, and SSSPM 0828 only does at the blue edge. SDSS 0539 and 2MASS 0559 show many correlated bins in this band, suggesting that there is intrinsic water variability in at least these latter two targets. There is also methane band in the region 1.31–1.49 μm, so in principle the variability could be due to this. This is plausible for 2MASS 0559, which is a T5 dwarf according to Burgasser et al. (2000), but perhaps even for SDSS 0539 (an L5 dwarf according to Fan et al. (2000)) where we possibly see methane absorption (section 4.3).

5 SUMMARY AND CONCLUSIONS

I have monitored four UCDs with differential infrared spectrophotometry to look for evidence of correlated variability over timescales between 0.1 and 5.5 hrs.

Of the four targets monitored, three show significant evidence for positively correlated variations. In the L2 dwarf SSSPM 0828 the most significantly correlated bands lie between 1010 and 1070 nm, with the next most significant regions ($|\rho_{i,i'}| > 0.8$) coinciding with Fe, FeH, VO, KI and water. SSSPM 0828 also shows similar broad band correlation patterns (and lack thereof) seen in the L1.5V 2M1439 reported by BJ02 (observed from a different site with a different instrument). The other L2V monitored, 2MASS 0847, is devoid of any correlated variability. The T5 dwarf 2MASS 0559 shows well correlated ($|\rho_{i,i'}| > 0.8$) variability at 925–962 nm, 1347–1351 nm and 1434–1448 nm which is probably due to water, possibly also methane. The L5 dwarf SDSS 0539 is different from the other three sources in that it exhibits many more regions of correlated variability, larger correlation coefficients and some anticorrelated regions. The latter coincide with TiO and FeH features. Generally, however, the correlations in SDSS 0539 are quite broad band and cannot always be associated with specific features. This would be consistent with variations in the dust opacity.

I have demonstrated that the observed correlated variability is not due to OH lines nor to telluric (water) absorption. For example, much of the correlated variability in 2MASS 0559 and SDSS 0539 occurs at wavelength regions where there is little correlated variability in the direct (non-relative) reference star spectra.

In conclusion, this work provides good evidence for correlated variability in three of four ultracool dwarfs. It is intrinsic to the sources and is not the result of telluric variability or colour-dependent extinction effects (Bailer-Jones & Lamm (2003)) in the Earth's atmosphere (because the relative fluxes are formed over very narrow bands). The analysis does not require an estimate of the noise level (flux amplitude), although the estimation of confidence intervals does use an assumption on the shape of the noise distribution.

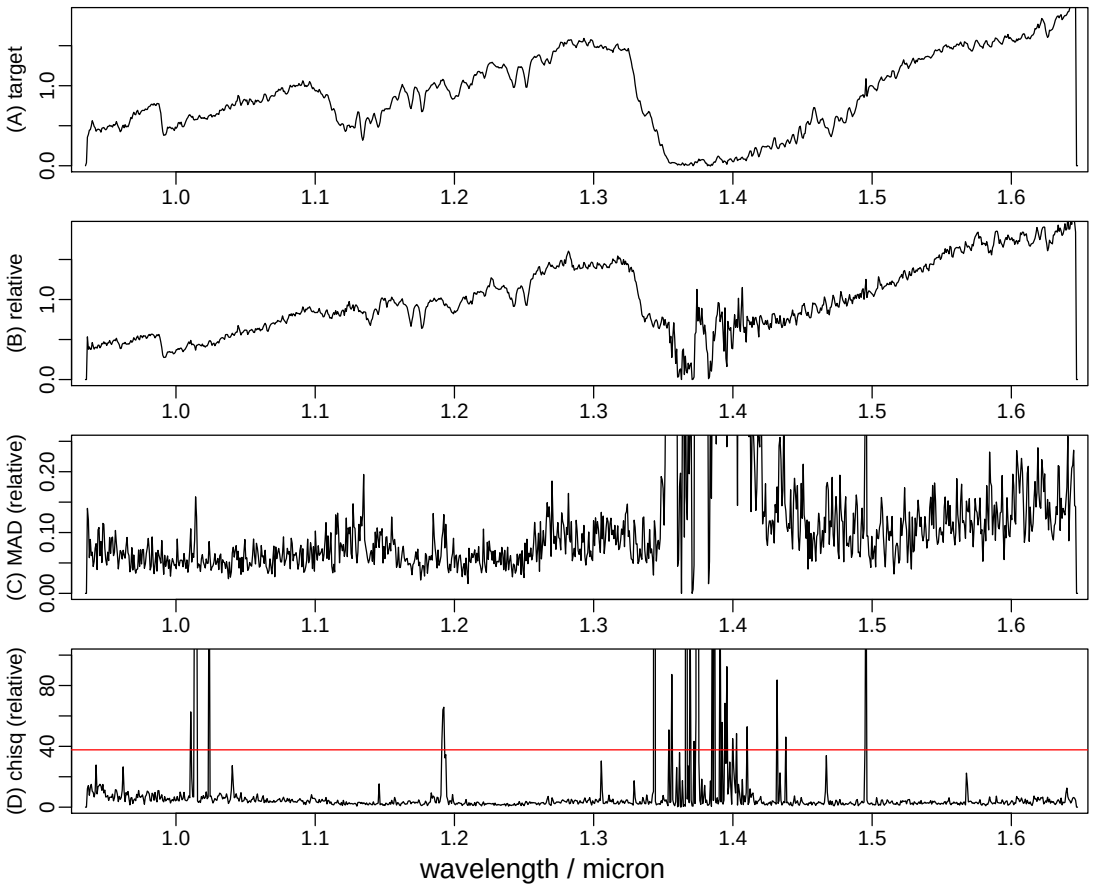

Figure 11. Spectra of the L5 dwarf SDSS 0539. See caption to Fig. 2

This multiband correlation analysis is more robust than single band analyses, because correlated variations are more likely to be intrinsic. This is not to say, however, that only wavelength-correlated variability in UCDs exists. Some variability is seen in narrow UCD features, such as the KI lines and FeH, CrH, TiO, but it is not limited to readily-identified spectral features. Much of the variability is broad band in nature, consistent with water and perhaps even methane, but also broader still, as would be expected by dust. Such a variety of elements and chemical phases in the variability signature suggests a common cause. A good candidate is local temperature and/or composition variations. The opacity is very sensitive to temperature, and local variations caused by rising convective columns of hot gas (for example), would change the relative ratios of molecular and gas species .

ACKNOWLEDGEMENTS

The data analysis and plotting in this article has made extensive use of the freely available R statistical package, http://www.r-project.org. I am grateful to its developers for the time and effort they have invested. I thank Viki Joergens, Bertrand Goldman and the anonymous referee for useful discussions and comments. The observations on which this work is based were obtained during ESO programme 072.C-0275.

REFERENCES

Allard F., Hauschildt P.H., Alexander D.R., Tamanai A., Schweitzer A., 2001, ApJ 556, 357
Bailer-Jones C.A.L., 2002, A&A 389, 963 (BJ02)
Bailer-Jones C.A.L., 2004, A&A 419, 703
Bailer-Jones C.A.L., 2005, in *Proc. 13th Cool Stars Workshop*, F. Favata, G.A.J. Hussain, B. Battrick (eds), ESA, SP-560, 429, astro-ph/0409463
Bailer-Jones C.A.L., Mundt R., 1999, A&A 348, 800
Bailer-Jones C.A.L., Mundt R., 2001, A&A 367, 218. Erratum: A&A, 374, 1071
Bailer-Jones C.A.L., Lamm M., 2003, MNRAS 339, 477
Burgasser A.J., Wilson J.C., Kirkpatrick J.D., et al., 2000, AJ 120, 1100
Burgasser A.J., Kirkpatrick J.D., Reid I.N., Brown M.E., Miskey C.L., Gizis, J.E., 2003, ApJ 58, 512
Chatfield C., 1996, The analysis of time series, 5th ed., Chapman & Hall, London
Clarke F.J., Tinney C.G., Hodgkin S.T., 2003, MNRAS 341, 239
Cruz K.L, Reid I.N., Liebert J., Kirkpatrick J.D., Lowrance P.J., 2003, AJ 126, 2421
Cushing M.C., Rayner J.T., Vacca W.D., 2005, ApJ 623, 1115
Enoch M.L., Brown M.E., Burgasser A.J., 2003, 126, 1006
Fan X., Knapp G.R., Strauss M.R., et al., 2000, AJ 119,

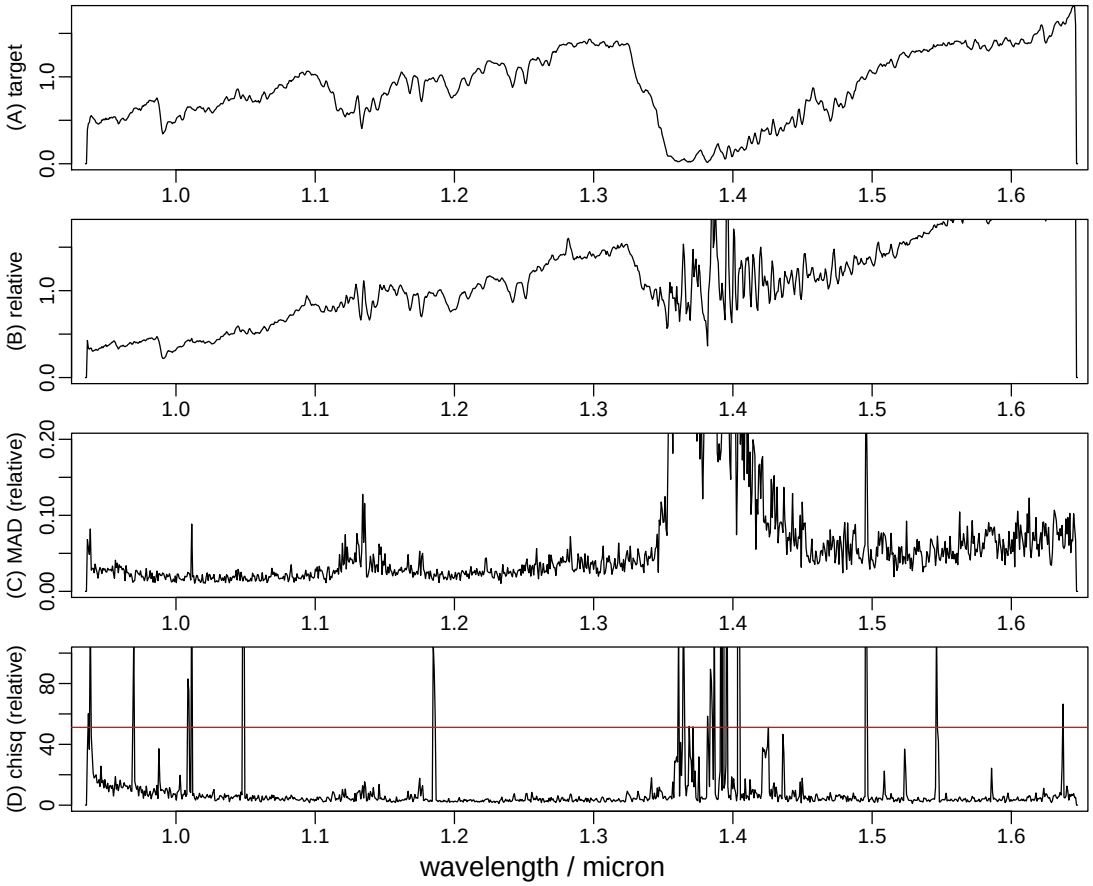

Figure 14. Spectra of the L2 dwarf 2MASS 0847. See caption to Fig. 2

928
Gelino C.R., Marley M.S., Holtzman J.A., Ackerman A.S., Lodders K., 2002, ApJ 577, 433 (G02)
Goldman B., 2005, Astron. Nachr. 326, 1059
Joergens V., Fernandez M., Carpenter J.M., Neuhäuser R., 2003, ApJ 594, 971
Kirkpatrick J.D., 2003, in ASP Conf. Ser. vol. 211, p. 189
`http://spider.ipac.caltech.edu/staff/davy/ARCHIVE/`
Koen C., Matsunaga N., Menzies J., 2004, MNRAS 354, 466
Lodders K., 1999, ApJ 519, 793
McLean I.S., McGovern M.R., Burgasser A.J., Kirkpatrick J.D., Prato L., Kim S.S., 2003, ApJ 596, 561
Mohanty S., Basri G., 2003, ApJ 583, 451
Nakajima T., Tsuji T., Maihara T., et al., 2000, PASJ 52, 87
Nakajima T., Tsuji T., Yanagisawa K., 2001, ApJ 561, L119
Oliva E., Origlia L., 1992, A&A 254, 466
Scholz R.-D., Mesuinger H., 2002, MNRAS 336, L49
Schweitzer A., Gizis J.E., Hauschildt P.H., Allard F., Howard E.M., Kirkpatrick J.D., 2002, ApJ 566, 435
Tinney C.G., Burgasser A.J., Kirkpatrick J.D., 2003, AJ 126, 975

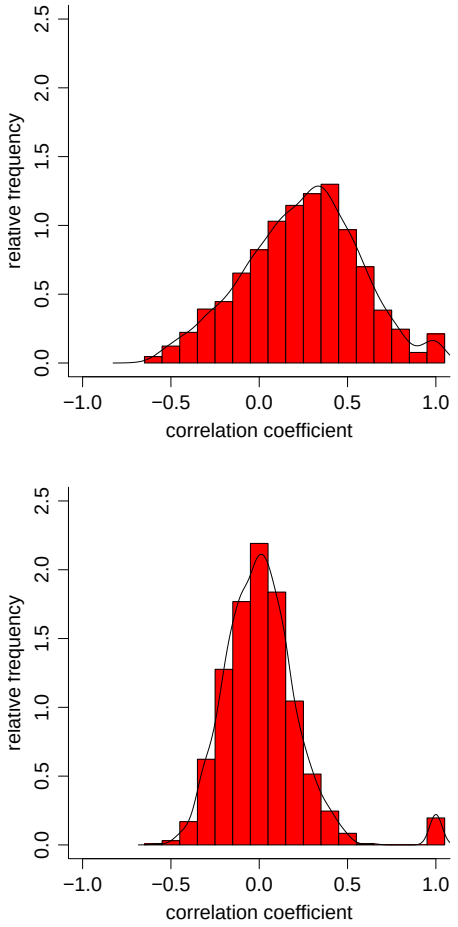

Figure 6. Histogram of the correlation coefficients for SSSPM 0828 (top; from Fig. 4) and for the random spectra (bottom; from Fig. 5). The ordinate is a density (i.e. the total area is 1.0). The overplotted line is a kernel density estimate.

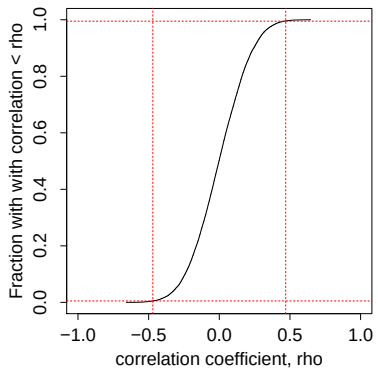

Figure 7. Limiting cumulative distribution of the correlation coefficients, $C(\rho_{i,i'})$, for the random spectra (Fig. 6, bottom), excluding the leading diagonal of unit correlations. The horizontal lines are at 0.005 and 0.995, i.e. there is only a 1% chance that the correlation coefficient could lie outside these limits for random data. The limits are $\pm$ 0.46 in this case ($S = 30$).

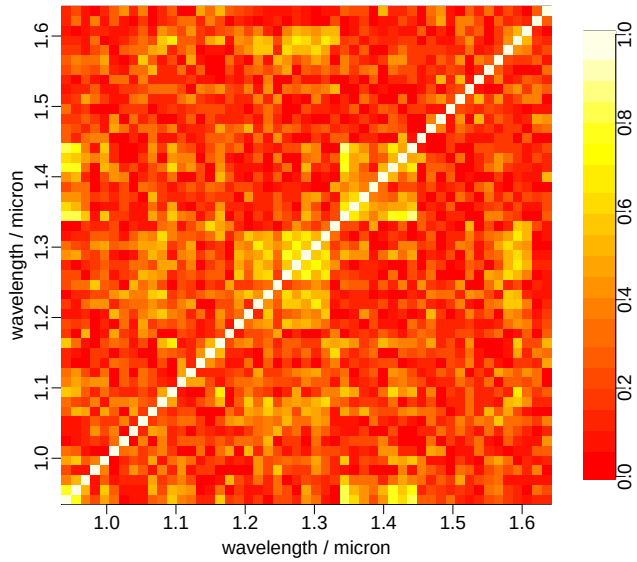

Figure 9. Correlation matrix for the relative spectra of 2MASS 0559 with a binning factor of 20. The absolute values of the correlation coefficients are shown.

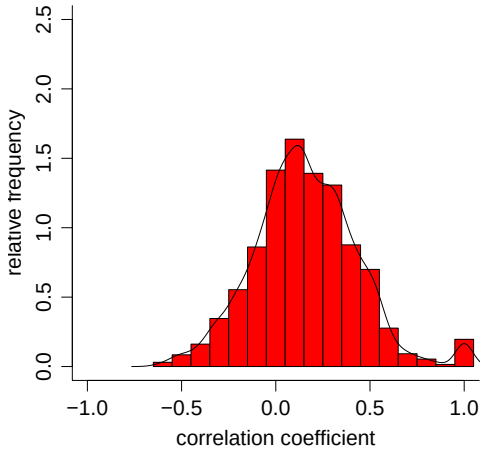

Figure 10. Histogram of the correlation coefficients for 2MASS 0559 from Fig. 9.

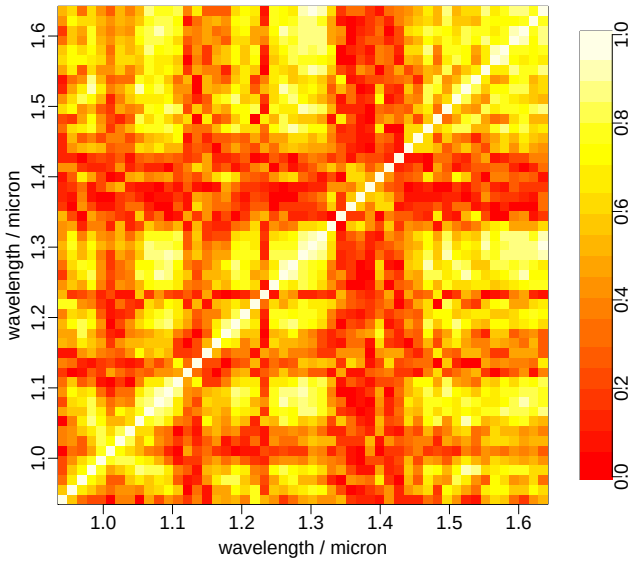

Figure 12. Correlation matrix for the relative spectra of SDSS 0539 with a binning factor of 20. The absolute values of the correlation coefficients are shown.

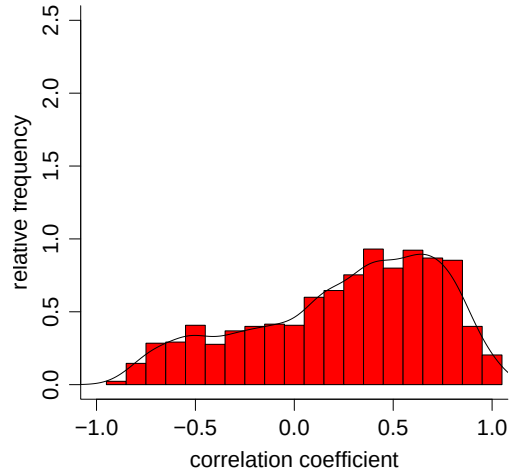

Figure 13. Histogram of the correlation coefficients for SDSS 0539 from Fig. 12.

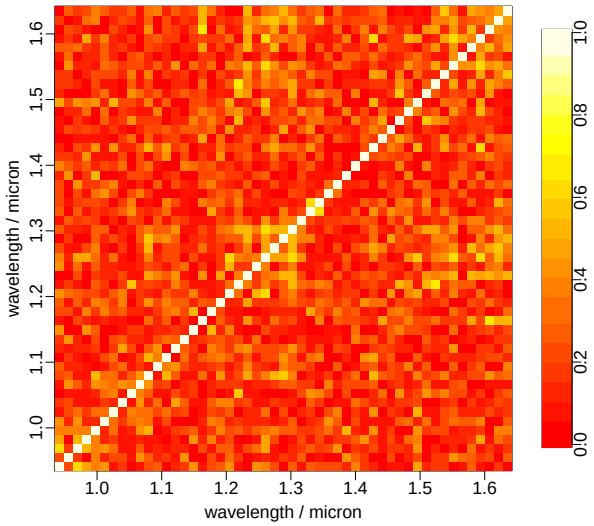

Figure 15. Correlation matrix for the relative spectra of 2MASS 0847 with a binning factor of 20. The absolute values of the correlation coefficients are shown.

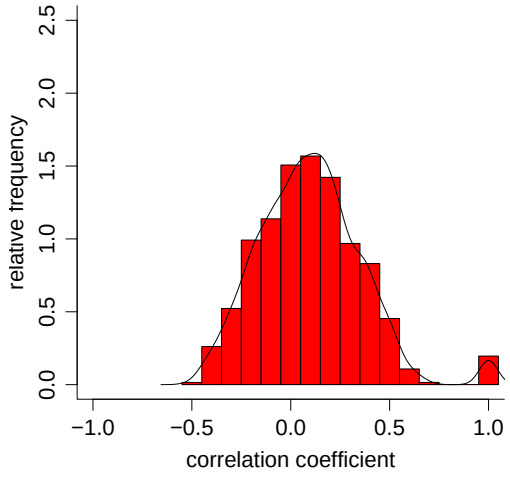

Figure 16. Histogram of the correlation coefficients for 2MASS 0847 from Fig. 15.